
This is an electronic reprint of the original article.
This reprint may differ from the original in pagination and typographic detail.

Kaljunen, Juho Uzkurt; Yazdani, Roza; Al-Juboori, Raed A.; Zborowski, Charlotte; Meinander, Kristoffer; Mikola, Anna

Adsorptive behavior of phosphorus onto recycled waste biosolids after being acid leached from wastewater sludge

Published in:
Chemical Engineering Journal Advances

DOI:
[10.1016/j.ceja.2022.100329](https://doi.org/10.1016/j.ceja.2022.100329)

Published: 15/08/2022

Document Version
Publisher's PDF, also known as Version of record

Published under the following license:
CC BY-NC-ND

Please cite the original version:
Kaljunen, J. U., Yazdani, R., Al-Juboori, R. A., Zborowski, C., Meinander, K., & Mikola, A. (2022). Adsorptive behavior of phosphorus onto recycled waste biosolids after being acid leached from wastewater sludge. *Chemical Engineering Journal Advances*, 11, Article 100329. <https://doi.org/10.1016/j.ceja.2022.100329>

This material is protected by copyright and other intellectual property rights, and duplication or sale of all or part of any of the repository collections is not permitted, except that material may be duplicated by you for your research use or educational purposes in electronic or print form. You must obtain permission for any other use. Electronic or print copies may not be offered, whether for sale or otherwise to anyone who is not an authorised user.



Adsorptive behavior of phosphorus onto recycled waste biosolids after being acid leached from wastewater sludge

Juho Uz Kurt Kaljunen^{a,*}, Roza Yazdani^b, Raed A. Al-Juboori^a, Charlotte Zborowski^c, Kristoffer Meinander^c, Anna Mikola^a

^a Department of Built Engineering, School of Engineering, Aalto University, Aalto FI-00076, Finland

^b Department of Mechanical Engineering, School of Chemical Engineering, Aalto University, Aalto FI-00076, Finland

^c Department of Bioproducts and Biosystems, School of Chemical Engineering, Aalto University, Aalto FI-00076, Finland

ARTICLE INFO

Keywords:

Phosphorus recovery
Adsorption
Biochar
Lignin
Sludgechar
Humic extract

ABSTRACT

A vast amount of phosphorus is being wasted or inefficiently utilized in wastewater treatment sludge worldwide. This paper investigates the adsorptive loading of phosphorus from the sludge on different biosolid materials for potential recovery and after use. The phosphorus was leached with acid from wastewater sludge from a chemical P removal process and adsorbed onto four different waste-based biosolid materials. The four biosolids were biochar, commercial lignin, sludge char (pyrolyzed wastewater treatment sludge), and humus (extracted from black liquor). Among the studied biosolids, loaded sludgechar had the highest phosphorus content, yet all materials performed well in P-adsorption. Optimal leaching and adsorption conditions were identified as pH 3 and adsorbent dosage between 0.5 g/L and 0.61 g/L for all biomaterials. The highest adsorption capacity value reached 400–500 mg/g with temperature-dependence. Biosolid materials were characterized with FT-IR, SEM-EDS, XRF, XRD, and XPS. Mathematical modeling through kinetic adsorption models showed that all biomaterials obey a pseudo first order kinetic model, and pore and intra-particle diffusion contribute to the adsorption mechanisms. The isotherm models suggest that the adsorbents are heterogeneous, and the adsorbate physiochemically bond with the functional groups of adsorbents with different adsorptive energies. The process is temperature-dependent and endothermic. XPS and XRD analyses showed that phosphorus adsorbed on the materials is mostly phosphate bound with Fe and Ca. Overall recovery efficiency was 21% (P bound on biosolids / P in sludge before leaching). Such phosphorus-loaded biomaterials are promising for use as feasible slow-release fertilizers.

1. Introduction

Phosphorous (P) recovery is important because it is a limited resource, and it is valuable for the growth of living organisms as well as different industries. The limitation of such an important resource might also cause political conflict in the future [1–5]. Wastewater treatment sludge has a high P concentration, but its recycling is problematic due to issues related to pollutants, hygienic concerns, and economic feasibility [6].

The main use for P is as a fertilizer [5, data from 7]. Excessive use of fast-release fertilizers causes the leaching of nutrients from agricultural soil, which has been identified as an environmental threat [8]. On the other hand, the fertilizing potential is difficult to determine precisely. Plant-available phosphate in fertilizers is typically measured with an

ammonium citrate solution [9,10]. However, a simple solubility test does not simulate the fertilizers' effect on plant growth [10,11]. Some recycled P fertilizers, such as struvite and vivianite, release P slower [12, 13]. The literature focusing on slow-release fertilizers presents the leaching of nutrients as the problem [14,15] and slow-release fertilizers as the solution [16–18]. These slow-release minerals are devoid of carbon, and soil health is strongly tied to their carbon content [19]. Soils even have the greatest potential for mitigating climate change [10, 20–22], and for these reasons, biosolids are an attractive option for the support structure for fertilizers.

This study explores a solution for P reclamation from chemical (Fe) wastewater sludge for fertilizer use. The four different biosolids we tested were biochar (BC), sludge char (SC), lignin (LI), and humus extract from black liquor (BL). BC represents a well-studied material [23–25], and the other three targeted biomaterials (SC, LI, and BL) are

* Corresponding author.

E-mail address: juho.uzkurtkaljunen@aalto.fi (J.U. Kaljunen).

Nomenclature for adsorption models (Section 2.6)

ΔG°	gibbs free energy change	K_t	Toth isotherm constant
ΔH°	enthalpy in free energy change equations	k	equilibrium constant in free energy change
ΔS°	entropy in free energy change equations	k_1	pseudo first order rate constant
A	Koble-Corrigan isotherm constant	k_2	pseudo second order rate constant
A_t	equilibrium binding constant for the Temkin isotherm model	k_{ad}	adsorption energy constant in the Dubinin-Radushkevich isotherm model
a_K	Khan isotherm exponent	k_{ip}	intraparticle diffusion rate constant
a_{rp}	Redlich-Peterson isotherm constant	m	mass of the adsorbent
a_t	Toth isotherm constant	n_H	hill isotherm constant
B	Koble-Corrigan isotherm constant	n_{K-C}	Koble-Corrigan isotherm constant
B_{rp}	Redlich-Peterson isotherm exponent	n_F	adsorption intensity in the Freundlich isotherm model
B_t	Boyd's diffusion model	n_S	SIPS isotherm constant characterizing system heterogeneity
b_k	Khan isotherm constant	R	universal gas constant
b_t	Temkin isotherm constant	V	volume
b_s	SIPS isotherm constant related to the energy of adsorption	Q_o	estimated max coverage capacity for the Langmuir isotherm
C_e	equilibrium concentration	q_e	adsorption capacity at equilibrium
c	intraparticle diffusion model constant for the thickness of the boundary layer	q_m	maximum adsorbed amount in the SIPS isotherm
c_0	concentration at $t=0$	q_k	Khan isotherm constant
c_t	concentration at time t	q_s	maximum adsorption capacity in the Dubinin-Radushkevich isotherm
K_d	hill isotherm constant	q_{sh}	hill isotherm constant
K_f	adsorption capacity in the Freundlich isotherm model	q_t	adsorption capacity at time t
K_L	langmuir isotherm constant (ratio between adsorption and desorption rate)	T	temperature
K_{rp}	Redlich-Peterson isotherm constant	t	time
		t_T	Toth isotherm exponent

new possibilities with high potential. SC is pyrolyzed sludge and is already loaded with iron. Iron in the material could improve the P adsorption potential and turn SC into a valuable fertilizer. Lignin is a biopolymer that coexists with cellulose in trees and plants, and a large quantity of this by-product can be extracted from black liquor in the paper manufacturing process. Black liquor is a waste stream from the paper mill process; it is commonly burned for energy production. We hypothesize that the organic substances extracted from BL concentrates could have a higher value as a P adsorbent. Binding P onto a carbon source and using the resulting material as a fertilizer provides a pathway to recycle P from waste sources into a potential fertilizer while supplying soils with carbon that improves nutrient retention and soil health.

BC is a well-researched material in terms of its function as P adsorbent in wastewater treatment and its manufacturing possibilities [26–28,25], and several papers discuss BC utilization as P adsorbent and its use as fertilizer. For example, Khan et al. [18] produced BC pellets loaded with NPK nutrients to be used as fertilizers. Yao et al. [28] manufactured Mg-loaded BC that was used to stimulate grass growth from seeds to sprouts.

The research on LI applications in nutrient adsorbents is trending. Chen et al. [29] reviewed the current advances in the use of LI as a slow-release fertilizer. Other studies have focused on modifying lignin to improve P adsorption [30,31]. These publications have reported good results in manufacturing P-specific LI materials to adsorb P and use it as a slow-release fertilizer [32–34]. However, there is still a knowledge gap in understanding lignin's performance as P adsorbent compared to the more common and more novel bio-adsorbents within the same or similar experimental framework.

Studies using SC (generally char produced from municipal waste-activated sludge (WAS)) are scarce. Yang et al. [35] prepared char from WAS through modification with iron for P adsorption. However, we assume that the WAS in Yang et al. [35] was from an enhanced biological phosphorus removal (EBPR) process and as such did not include metals, which led to the modification requirement with iron for P adsorption. Other studies that used pyrolyzed WAS focused on sludge

disposal management and not for P adsorption.

To the best of our knowledge, there are no articles on the use of BL as P adsorbents in the existing literature. Instead, a few articles show that the presence of humic substances increases the bioavailability of P in soils [36,37]. Therefore, P adsorption on humic substances from BL is a knowledge gap that has been brought to light in this study. Furthermore, this study utilizes real wastewater treatment plant (WWTP) sludge as a P source. Thus, the results are novel since they reflect realistic conditions of the P source.

This study aims to uncover how the suggested biosolids perform for the adsorption of P that has been extracted from WWTP sludge by leaching and to identify the most optimal adsorbent. To understand the adsorption process, the authors utilized a variety of mathematical models to evaluate the kinetic, isothermal, thermodynamic, and diffusional behavior of P in these biosolids. A wide range of characterization methods was also harnessed to assess the characteristics of loaded biosolids and their feasibility for use as fertilizer. This study is linked to NPHarvest, another nutrient recovery project at Aalto University [38]. The goal of the project is to enhance wastewater treatment while recovering N and P in a sustainable manner. Thus, augmenting NPHarvest with P leaching and its adsorption on a carbon source is an attractive solution for P reclamation.

2. Materials and methods

2.1. Phosphorus source

The sludge where phosphorus was extracted originated from Viihkimäki WWTP in Helsinki, Finland. The WWTP is an enhanced nutrient removal plant with chemical P precipitation using ferrous sulfate and biological nitrogen removal. Ferrous sulfate is dosed in grit removal and in the aeration basin. WAS and raw sludge from the activated sludge process are thickened and digested together in mesophilic digesters and dewatered. The samples were collected after dewatering in autumn 2019 and stored at 4°C for several months. The annual average

characteristics of the dewatered sludge are dry matter 29%, total phosphorus 33 g/kgTS, calcium 28 g/kgTS, and iron 110 g/kgTS. The sludge also has low total heavy metal concentrations, reported by Helsinki Region Environmental Services (HSY). They used SFS-EN ISO 11885:2009 standard and ICP-OES method (for example, Cu 300 mg/kgTS, Pb 14 mg/kgTS, and Cd 0,27 mg/kgTS) [39,40].

2.2. Adsorbents

The biosolids, i.e., BC, LI, BL, and SC were used as powders in the adsorption tests. The materials represent commercially available products, side streams or waste flows and as such their manufacturing methods (e.g. temperature) were not the same. All materials were ground and sieved through an 80 μm mesh before using them as adsorbents. BC was produced via pyrolysis at 600°C from wood and was provided by Carbons Finland Oy. SC was acquired from the Helsinki Regional Environmental Services (HSY) pyrolysis pilot plant. The pyrolysis plant processes only municipal wastewater sludge (from the same plant as the sludge used in this study) at a temperature of 500°C and a residence time of 90 min. BL was provided by a pulp plant in Southern Finland. Organic material (or humus) extraction was adapted from Mema [41]. Briefly, the pH of 1 L of black liquor was decreased to 2 with 20% HCl and stirred for 4 h, followed by centrifuging to separate the solid fraction. The solid fraction was dissolved with 0.1 M NaOH and precipitated again with HCl several times to remove impurities. Finally, the solid material was dried, pulverized, and sieved. LI was provided by UPM-Kymmene Oyj.

2.3. Material characterization

Both loaded and unloaded biomaterials were analyzed with a range of measurements. Zeta potential analysis was used to study the surface charge of the adsorbents with pH and see if electrostatic interaction is a dominant mechanism. Malvern Zetasizer Nano ZS was used for measurements by a procedure similar to the one reported in [42,43]. A dose of adsorbent was added to deionized water and exposed to mixing and ultrasonication followed by a pH adjustment. The presence of P was analyzed by FT-IR scans taken with a PerkinElmer FTIR with ATR, 16 scans, and 32 cm^{-1} resolution. The morphology and the surface composition were studied using a scanning electron microscope with the energy-dispersive spectroscopy (SEM-EDS) model JEOL JIB-4700F with an accelerating voltage range of 3–5 kV and a current of 10 nA. To increase the conductivity of the powder specimens and obtain good quality images, the powders were coated with gold/palladium (Au/Pd). The elemental content of the adsorbents before and after adsorption was determined using an X-ray fluorescence (XRF) spectrometer (PANalytical (WD)XRF Axios mAX) and X-ray diffraction (XRD) PANalytical X'Pert Powder XRD for exploring the nature of crystal formation on the biosolids. The BET surface area, pore size, and volume of the adsorbents were quantified using the BELsorp Mini II. All samples were degassed at 110°C for 24 h.

X-ray photoelectron spectroscopy (XPS) measurements were carried out using a Kratos AXIS Ultra DLD spectrometer with an Al K α monochromatic X-ray source (1486.7 eV). Survey scans were taken with a 1.0 eV step and 80 eV analyzer pass energy, while high-resolution regional spectra were recorded with 0.1 eV step and 20 eV pass energy. During the measurements, the samples were charge-neutralized using slow electrons from a tungsten filament. The base pressure of the system was below 1×10^{-9} Torr. For each sample, XPS measurements were repeated three times on different points of the sample surfaces to check for homogeneity, reliability, and reproducibility of the results. The position of the acquired peaks was charge-corrected relative to the position of the C 1s component for C-C bonding at 284.8 eV. Analysis of the XPS data was done with CasaXPS software. The purpose of the analyses was to observe and quantify the change in P between raw and loaded biomaterials, visually understand how P was bound on adsorbents, and measure the

porosity and surface area of the adsorbents.

2.4. Phosphorus leaching and adsorption procedure

P was leached from the sludge by placing X g of sludge described in Section 2.1 and 1 L water (ratio was selected based on preliminary testing) into a large beaker and mixing at 400 RPM for 6 h. pH was decreased with strong sulfuric acid to the desired level. Then the solution was centrifuged and filtered through a GF/A and 0.45 μm filter combination, where a rougher GF/A filter was placed on top of a 0.45 μm filter to stagger the cake formation and decrease resistance build-up.

Adsorbing tests were conducted less than 24 h after leaching since leachate could not be stored longer than a few days before a sulfate precipitate started to form. An adsorbing test was conducted as batches by weighing a certain mass of adsorbent (defined below) and measuring a certain volume of leachate into a shaker flask (defined below). The flask was in the shaker for 24 h for the first optimization tests and 96 h for the following kinetic, isotherm, and temperature tests. Afterward, the loaded adsorbent was separated by filtering. The performance of the test was evaluated by analyzing orthophosphate (PO_4^{3-}) and total phosphorus (TP) while the adsorbent was dried and examined with various characterization analyses.

Optimal pH and dosing for the adsorption process were investigated by ranging the leaching pH from 3 to 5 and the dosing value from 0.5 to 2 g/l. The sludge-to-water ratio was 60 g/l, shaker flask size 50 ml, contact time 24 h, and temperature 20°C. Design Expert 9.0 software was used to perform optimization of the adsorbent dosage and solution pH using response surface methodology (RSM). Central composite design (CCD) was applied to study the effect of tested factors (pH and adsorbent dosage) on phosphorous adsorption. The desirability function of RSM was utilized to conduct multi-response optimization to identify the best levels of the examined factors. Afterward, the optimized values of pH and adsorbent concentration were applied in the subsequent adsorbent experiments. The optimization results will be discussed in detail in Section 3. For the kinetics test, adsorption experiments were conducted with a 300 ml flask to offset the liquid volume loss when extracting samples during the test. Adsorption isotherm tests were performed by leaching sludge with a loading of 30, 60, 90, 120, and 150 g/l to produce leachates with different P concentrations. Temperature tests were conducted at 10, 20, 30, and 40°C, respectively.

2.5. Total phosphorous and phosphate measurements

Orthophosphate and total phosphorus were analyzed from liquid samples with a method based on SFS 3026, dated 1986. The equipment used was both the Shimadzu UV-1800 and Skalar BluVison Analyzer spectrophotometers with $\lambda=880$ nm and a 1 cm cuvette. P-loaded solid materials were analyzed in a similar manner as the raw biosolids were characterized.

2.6. Adsorption process

The models that the authors used are shown in Supplementary Materials (SM) Table SM1 for kinetic, isotherm, temperature, and diffusion models. Table SM1 includes equations and reference numbers for the used models. The initial parameters for the iteration of the fitting algorithm for the kinetic, isotherm, temperature, and diffusion models were estimated using values presented in the literature, such as the study by Rezakazemi and Shirazian [44]. The fitting was performed using the Origin lab nonlinear function (NLF), which utilizes the Levenberg–Marquardt algorithm. The adsorption capacity is calculated according to Eq. (1).

$$q_t = \frac{(c_0 - c_t)V}{m} \quad (1)$$

Where q_t is the adsorption capacity, c_0 is the initial concentration of

the substance in solution, c_t is the concentration of the substance in the solution at contact time t , V is the volume of the solution and m is the mass of the adsorbent.

For the kinetic studies, two models—pseudo first and second order (PFO and PSO, respectively)—were tested to study the phosphate and total phosphorus removal rate by fitting experimental data against the theoretical model. The PFO model uses Eq. (S2) [45]. PSO uses Eq. (S3) [46] and assumes that the process goes by the second order uptake when considering the surface sites of the adsorbent.

For the isotherm studies, to study the effect of the adsorbate/adsorbent concentration on the adsorption process, approximate correlations for equilibrium curves were found by using adsorption isotherms. The experimental data was fitted with isotherm models (Eqs. (S4) to (S13)) to understand the behavior of different adsorbents and P during the adsorption process.

The Langmuir isotherm model (Eq. (S4)) assumes monolayer adsorption on a homogenous surface with all adsorptive sites having equal affinity towards the adsorbate [47]. The Freundlich isotherm model (Eq. (S5)) is an empirical equation that has been applied for multi-layer adsorption on heterogeneous surfaces [48]. The Temkin isotherm model (Eq. (S9)) assumes that the heat of adsorption in a layer decreases linearly rather than logarithmically. It contains a factor for taking the adsorbent-adsorbate interaction into account [49,50].

The Redlich-Peterson (R-P) isotherm model (Eq. (S6)) is an empirical formula combining the Langmuir and Freundlich isotherms into a three-parameter model. The presence of both heterogeneous and homogenous surfaces is assumed [48]. Similar to R-P, SIPS (Eq. (S7)) is also a hybrid Langmuir and Freundlich combination model [48]. Among the three-parameter monolayer models, it is considered the most applicable for explaining adsorption [51,52]. The Koble-Corrigan isotherm model (Eq. (S12)) is similar to SIPS and R-P in that it is a three-parameter model that combines the Langmuir and Freundlich models [49]. The Hill isotherm model (Eq. (S10)) aims to describe the binding of different species onto homogenous adsorbates while assuming that adsorption is a cooperative phenomenon [53,54].

The Dubinin-Radushkevich (D-R) (Eq. (S8)) isotherm model considers the porosity of the adsorbents by assuming that the adsorption process works through micropore filling rather than layer-by-layer adsorption on pore walls. It also does not consider the constant adsorption potential or the homogenous surface [55]. Hu and Zhang [55] noted that the $1/C_s$ term should be C_s/C_e , where C_s is the solubility of the adsorbate. This was not applied in this study due to the uncertainties related to the solubility of P in the experimental setup. Determining solubility would require a species of precipitate that was not present in the study [56]. The Toth isotherm (Eq. (S11)) model was developed to improve Langmuir fittings and is an empirical model [49]. It has proven useful when describing heterogeneous systems, and asymmetrical energy distribution is assumed [57,58]. The Khan isotherm model (Eq. (S13)) is proposed for pure solutions [59].

The adsorption temperature effects and the thermodynamic behavior of the process were analyzed from the free energy change described in Eqs. (S14) and (S15) [60]. The values of $\ln k$ were taken from the intercept of the plots of $\ln(q_e/C_e)$ vs. q_e . Furthermore, two adsorption diffusion models were included. The adsorption reaction usually happens in different phases: (1) the movement of molecules from solution to the surface (surface layer formation), (2) their movement from the surface towards the pores (the diffusion layer), and (3) their spreading out in the pores (intra-particle diffusion) [61]. The intraparticle (Eq. (S16)) [62] and Boyd (Eqs. (S17) and (S18)) [63] models were used to understand the balance between these mechanisms [47]. El-Khaiary and Malash [63] made a notion that the Boyd equations have been used incorrectly in publications. They are both shown in Table 4, but the majority of the data in this study falls under the conditions $q_t/q_e < 0.85$, and therefore Eq. (S18) was used.

2.7. Mild acid extractable P

Mild acid extractable fraction of P in the loaded biosolids produced in the temperature test was tested with method adapted from Wang et al. [64]. The loaded biosolids from all four temperature tests were mixed together, respectively. 0.35 g of loaded biosolid was placed in a 50 ml Erlenmeyer flask with 35 ml of 2% citric acid. The flask was shaken for 30 min. The contents were centrifuged for 15 min at 10 000 RPM with Hermle 2366K centrifuge and filtered with Macherey-Nagel 640W filter paper (art. nr. 202 009). PO_4^{3-} was analyzed from the liquid fraction and compared to the amount of P bound in the loaded biosolid in the adsorption test. All extraction tests were replicated.

3. Results and discussion

The results show the adsorption efficiency for the tests conducted, the mathematical model fitting results, and the loaded and unloaded biosolid characterization results. The results are presented only for PO_4^{3-} . Both TP and PO_4^{3-} were measured, but in all cases, 98–99% of TP was in the PO_4^{3-} form, and thus the results are very similar. The overall recovery efficiency consists of both the efficiency of P leaching from the sludge and the following adsorption efficiency on biosolids. The P leaching efficiency was 47%, 36%, 42%, 27%, and 25% for sludge dosing of 30 g/l, 60 g/l, 90 g/l, 120 g/l, and 150 g/l, respectively (calculated as fraction of P that dissolved from sludge during the leaching test). Fig. SM1 shows the isotherm test results. The adsorption efficiency was calculated by $100 \cdot (c_0 - c_e) / c_0$ where c_0 is the initial P concentration and c_e is the final P concentration in the adsorption test. The adsorption efficiency achieved in this study varied between 45% and 84% depending on the concentration of adsorbent and biosolid. The adsorption efficiency values were obtained from both kinetics test (Section 3.3) and isotherm test (Section 3.5). The maximum combined recovery efficiency reached in this study was 21%. The combined efficiency was calculated as the fraction of P from raw sludge was bound on the biosolid. The tests that produced results for the efficiency calculation above were performed in room temperature. The leaching process was expected to release a variety of substances due to the P origin being real wastewater treatment sludge from a WWTP. Iron was measured from the liquid phase since the sludge contained a high iron concentration. The leachate samples throughout the study had a soluble iron concentration of 1000 ± 300 mg/l.

3.1. The effect of pH

The Zeta potential is shown in Fig. 1, within the pH range used for the optimization step of this study. The potential is negative but increases towards pH 2, with SC having the lowest absolute potential value and LI the highest. When pH decreases, the surface becomes less negatively charged, and that can cause repulsive forces towards negatively charged molecules (such as phosphate) to decrease. This is supported by higher P adsorption at pH 3. pH 3 was the lowest point tested in the adsorption tests since the authors considered acid consumption to be economically unfeasible if leaching (and the following adsorption) was performed at pH below 3. The surface responses in Fig. 2 show a decrease in the surface response between pH values of 4 and 5, which is also consistent with the decrease found in the zeta-potential data (Fig. 1) for BC, SC, and BL. This suggests that the electrostatic interaction might play a role in PO_4^{3-} adsorption.

In addition, the leaching process is more efficient at lower pH values. pH 3 leachate has a higher P concentration than pH 5 leachate. We tested adjusting pH upwards between the leaching and adsorption tests, but P-metal compounds precipitated instantly. This phenomenon was out of the scope of this study since we wanted to study adsorption on biosolids, and therefore the pH adjustment prior to adsorption was not investigated further.

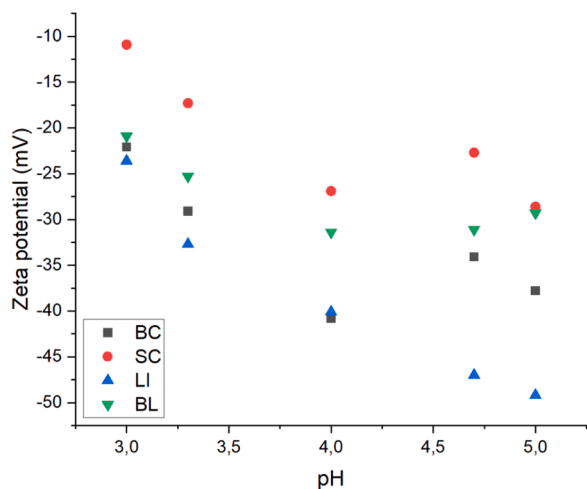


Fig. 1. Zeta potential for the biomaterials. The values are averages provided by the analysis equipment. The selected pH values were 3, 3.3, 4, 4.7 and 5. The standard deviation error bars are excluded to enhance readability. A figure with error bars is presented in Fig. SM1.

3.2. The effect of adsorbent dosing, surface area, and porosity

The surface responses plots in Fig. 2 show a similar behavior from all four biosolids. The goal of the surface response analysis was to find optimal test conditions for further tests rather than produce a model with a perfect fit. ANOVA for the surface response quadratic model (shown in Table SM2a and b) showed a significant lack of fit. However, other assessment criteria were satisfactory. Thus, the authors were satisfied enough with the optimization results to proceed with further

tests. A desirability analysis was performed based on the surface response (also shown in Fig. SM2) with the aim of maximizing the q value. The desirability outcome showed that the optimal conditions for all materials are pH 3 and adsorbent dosage of 0.61 g/l for BC, 0.5 g/l for SC and LI, and 0.52 g/l for BL. Higher adsorbent dosing concentrations decrease the specific amount of adsorbed P due to the inverse relationship presented in the Eq. (1). In addition, higher adsorbent dosing may lead to the agglomeration of adsorbent particles in the shaker flask, especially in acidic environment [65]. This can prevent P from reaching the active sites on the biosolid, decreasing the q value.

The BET analysis results for surface area and porosity are shown in Table 1. Among the studied solids, BC shows the highest surface area, and SC shows a notable pore volume. Despite the significant variation in the physical structure of the adsorbents, they all resulted in approximately the same adsorption capacity. This indicates that porosity and surface area may have little influence over P adsorption for the tested materials. Deng et al. [32] compared Mg- and Al-loaded biochar to pristine BC. While the loaded materials had a higher porosity and larger surface area, the higher P adsorbing efficiency was mainly credited to other effects, such as precipitation and anion intercalation. The importance of surface area or functional sites depends on the target pollutant, which justifies the need for tailoring new materials based on the target pollution or application. For instance, pollutants like phosphate require active sites to bond with the surface, but pollutants such as organic matter need a high adsorptive surface area [23,24]. This would indicate that the impact of active/favorable binding sites overpowers the larger surface area that higher porosity offers.

3.3. Kinetic study

The kinetics tests were performed using the optimized pH and dosage values. The results are shown in Fig. 3. The authors extended the contact

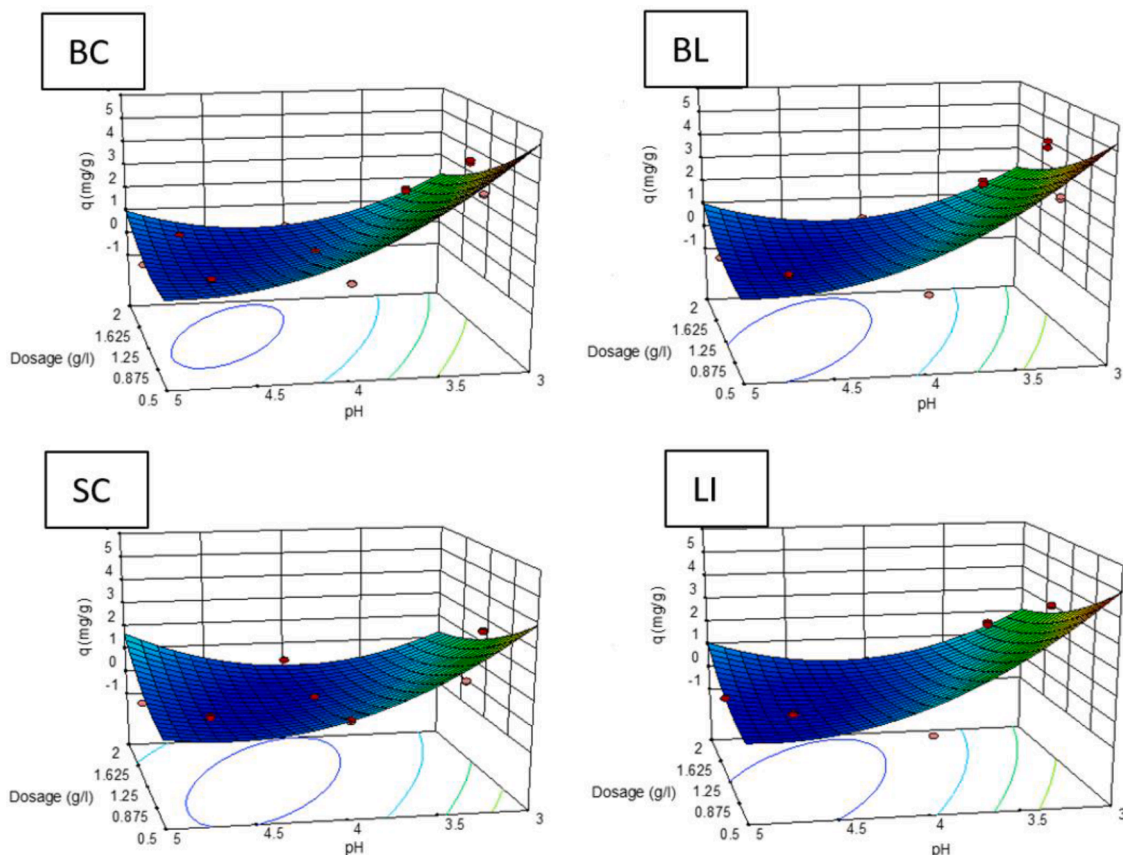


Fig. 2. Surface response plots for the optimization test in terms of PO43-.

time to 96 h to reach equilibrium in the system. SC shows a better adsorbing capacity than the rest of the materials, while BC shows the lowest capacity. The equilibrium is reached in about 70 h. Among the studied materials, SC showed the highest adsorption capacity, reaching up to 50 mg/g, while the rest also showed very good q_e , reaching up to 40 mg/g of capacity. This can again infer that surface area may not play the dominant role in P adsorption as functional groups. SC, LI, and BL most likely have a more active surface as their unloaded materials have higher mass fractions of metals (Fe, Ca, Al, S) compared to pure BC, which is discussed in later sections.

The experimental kinetics data were examined with the pseudo first and second order kinetics models (Eqs. (S2) and (S3)). The fittings results are presented in Table 2. The graphical representation for BC is provided in Fig. SM3. The R^2 values for BC are 0.96 for PFO and 0.94 for PSO models, indicating that PFO is a better fit. Similar behavior was observed for all biosolids, so the reactions mainly follow pseudo first order kinetics. The study by Arun et al. [66] found similar results (0.97 for PFO and 0.96 for PSO) for the adsorption of several chemical species on their BC. Wang et al. [67], on the other hand, reported that the PSO model produced a better fit for BC impregnated with Ca for adsorbing P, but their pure BC had R^2 values of 0.987 and 0.992 for PFO and PSO, respectively. Thus, we assume that the presence of several chemical species in the solution yields P adsorption that favors PFO. This conclusion is supported by Li and Shi [68]. They conclude that phosphate adsorption is described better by PFO when adsorption occurs simultaneously with ammonia and tetracyclin.

3.4. Diffusion model fits

If intraparticle diffusion is the controlling mechanism in the process, then the model fit is a straight line. The model fits are shown in Fig. 4, and their respective R^2 values are tabulated in Table 3. All model fits demonstrated improved R^2 value after the piecewise linear fit, but the impact was more significant for LI and SC, while BC and BL had only a slight increase. This suggests that P adsorption onto BC and BL is mainly controlled by intraparticle diffusion, while for LI and SC, it is likely affected by other processes as well. Intraparticle diffusion is the main rate-controlling step if the fitted line goes through the origin. While the line of each biosolid is close to the origin (intercepts for the single linear fit being -0.96 ± 1.75 for BC, -2.96 ± 3.55 for LI, -2.90 ± 3.92 for SC, and -4.93 ± 2.80 for BL), it cannot be determined if they pass through it. This conclusion is supported by the Boyd model fits, shown also in Fig. 4

and Table 3, which have high R^2 values (0.99 for BC, 0.92 for LI, 0.97 for SC, and 0.99 for BL), which indicates that pore diffusion has a role in the adsorption process. The fits in the Boyd model do not cover an equal length due to the mathematical nature of the model. After reaching equilibrium, the term B_t become an undefined value

3.5. Isotherm study

Increasing P concentration in the leaching phase does increase the P yield up to a point. A 90 g/l sludge dosing corresponds to an equilibrium adsorption capacity of 250–300 mg/g, and it provides a significant increase to the adsorption capacity compared to 30 g/l and 60 g/l sludge dosing (approximately 50 mg/g and 150 mg/g equilibrium adsorption capacity, respectively). On the other hand, 120 g/l and 150 g/l sludge dosing provided only a minor increase. A graphical result for the isotherm test is shown in Fig. SM4. Sludge char showed the highest P binding capacity, which can be due to higher metal oxide content present in its structure and thus plentiful binding sites for P.

The isotherm model best fit was determined by the R^2 value as well as the shape of the curve. The isotherm curve can be favorable, linear, or unfavorable. A curvature that extends to infinity is considered unfavorable, whereas a curvature that approaches a certain limit is favorable [69]. This is intuitive since an adsorption system should find equilibrium. The fits are presented in Fig. 5 and fit parameters in Table SM3. The best fits for both R^2 value and shape were SIPS (0.95) and Hill (0.94) for BC; SIPS (0.97), Hill (0.97), and R-P (0.98) for BL; SIPS (0.97), Hill (0.97), and R-P (0.98) for LI; and R-P (0.96) for SC. The behavior of SC was the most difficult for the models to predict, possibly due to its complex surface chemistry.

The Hill isotherm model showed a good shape and high fit for all biomaterials except SC. Even for SC, Hill was the second-best fit, with an R^2 value of 0.82. Originally proposed by Koopal et al. [70], for the non-ideal competitive adsorption (NICA) model, the Hill isotherm works for modeling the binding of different species onto homogenous material. This applies to this study since the leachate contains several chemical species due to its origin from real sludge. The presence of multiple species can be the reason for Langmuir and Freundlich's poor performance since they were developed for a single solute. According to Ringot et al. [71], the term n_H describes the cooperativity of the binding of species. If $n_H > 1$, there is positive cooperative binding. This value is higher than 1 for all biomaterials, indicating that the binding phenomena are cooperative. Iron that was also leached from sludge is possibly

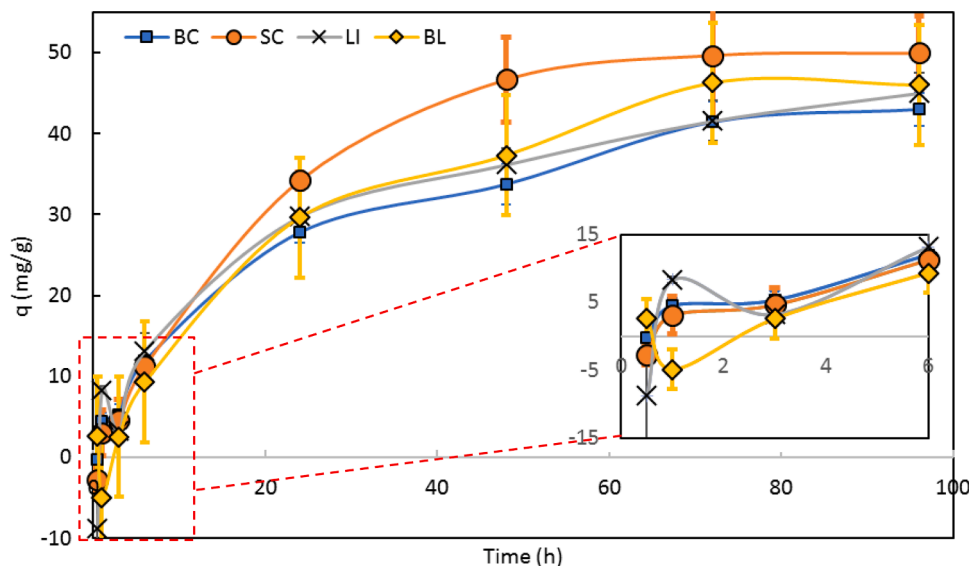


Fig. 3. Adsorbing kinetics for PO43-. Lines are added to enhance readability. The authors do not apply any models in this graph. The embedded plot shows the first 6 h of the test.

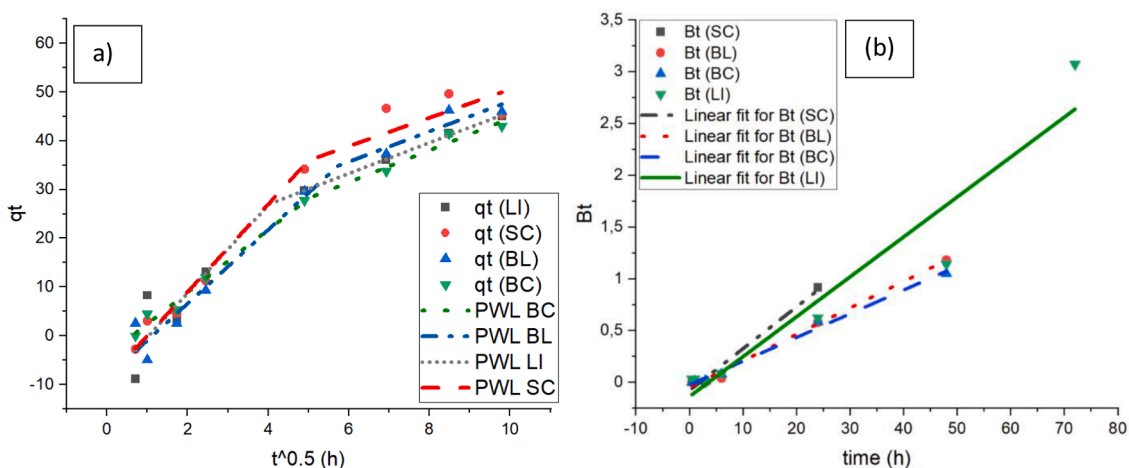


Fig. 4. Model fits for (a) intraparticle diffusion with the piecewise linear fit and (b) Boyd.

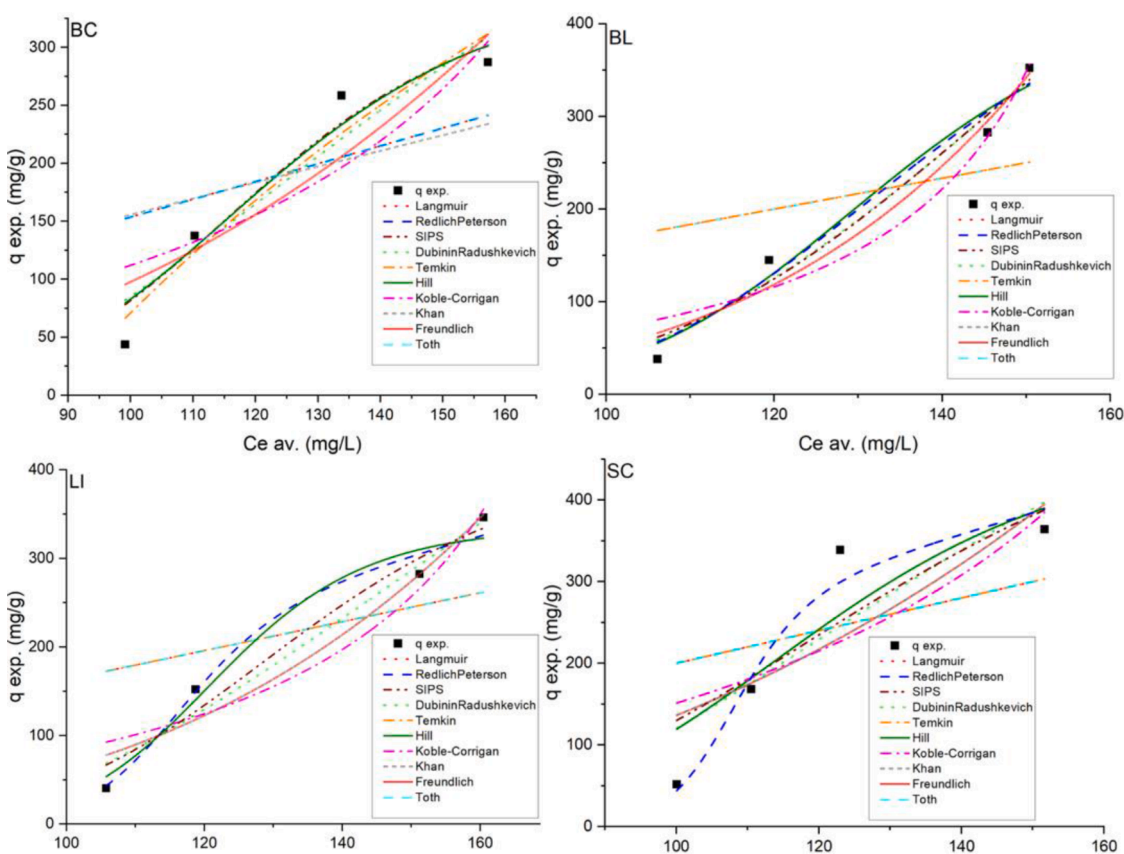


Fig. 5. Isotherm model fits for all biosolids.

bound on biomaterial as well, aiding the P binding, which is confirmed by the XPS and XRD results later in the discussion.

The R-P isotherm model produces a good fit for all biomaterials except BC. This model is also applicable to heterogeneous systems [72], such as the one in this study. Gimbert et al. [72] also showed that the term β_{rp} should be between 0 and 1 since it controls whether the equation is Henry's law ($\beta_{rp} = 0$), the Freundlich model (K_{rp} and $a_{rp} \gg 1$, $\beta_{rp} = 1$), or the Langmuir model ($\beta_{rp} = 1$). These constraints make the R-P model results questionable, particularly with the limited number of experimental data points used in this study. $\beta_{rp} \ll 1$ for SC, LI, and BL, which does not correspond to using the model correctly. Therefore, while the model provides a mathematically good fit, it may not represent

a realistic scenario.

The SIPS isotherm model had a high fit and relatively good shape for all materials except SC. SIPS is analogous to R-P, a combination of the Langmuir and Freundlich models. It describes adsorption onto heterogeneous surfaces and estimates the monolayer adsorption capacity at high sorbate concentrations [73]. The b values (indicating the energy of adsorption) for all biomaterials are considerably lower than those reported in other P sorption studies, while q_m values are considerably higher [73]. However, as this study utilizes heterogeneous, non-synthetic materials, the differences are expected.

The isotherm models with a mathematically good fit but unfavorable shape were Temkin and D-R for BC and Freundlich, D-R, Koble-Corrigan,

and Khan for both LI and BL. Their shape was on the linear or exponential side. These results suggest that the studied adsorbents provide heterogeneous surfaces with energetic differing active sites for P adsorption, and the used leachate contains several co-existing species, which cannot be reflected well by these models. Instead, as three-parameter models (apart from Temkin and Freundlich), they give

more mathematical freedom to fit the model to the data.

3.6. Temperature effects

The effect of temperature on P adsorption on the four tested adsorbents is shown in Fig. SM5. The thermodynamic parameters of P

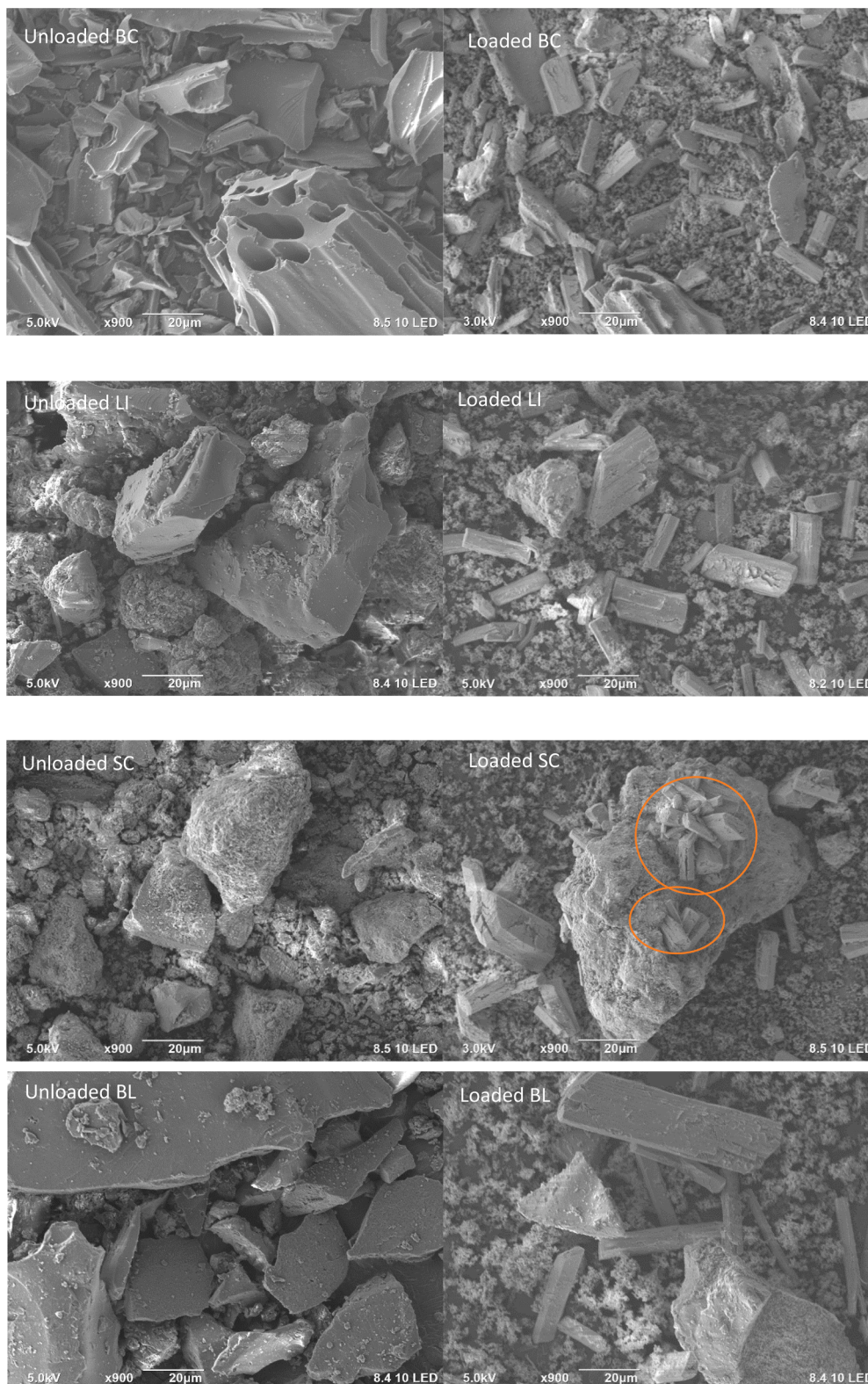


Fig. 6. SEM images for all unloaded and loaded biosolids. Crystal growth on SC particles is highlighted with orange circles.

adsorption onto the four adsorbents are presented in Table 4. All four materials behaved similarly, with BC performing slightly worse than other materials and SC having the highest variance. ΔG^0 is negative and decreases when temperature increases. ΔH^0 is positive for all materials, indicating that the adsorbing reaction is endothermic, and thus, higher temperature provides a better yield. ΔS^0 is negative, meaning that the entropy of the system decreased during adsorption. The decrease in ΔG^0 values indicates an increasing trend in the intensity of the adsorption process. Thus, higher temperature increases the P yield, which is in line with previous studies focusing on BC [32,74].

3.7. Characterization and P detection on loaded biosolids

A variety of characterization methods were employed to examine the biosolids before and after adsorption. SEM-EDS were utilized to study the change in surface morphology and composition of adsorbents before and after P adsorption. Fig. 6 shows the SEM images of unloaded and loaded biosolids. The EDS mass fractions and spectrums are presented in Table SM4 and Fig. SM6, respectively. From the images, it is clear to see that only BC is a porous material, which confirms the result of the BET analysis. The P fraction in loaded biosolids increased significantly for BC, LI, and BL. The SC P fraction increased as well. However, the unloaded SC contained P to begin with, so the increase is less significant. The loaded SC has crystal formation on top of the biosolid particle, marked by orange circles in Fig. 6. The crystals formed are likely related to metal-phosphates structures or other structures (e.g. CaSO_4) that form on the biosolids. The other loaded biosolids maintain a similar particle shape as their unloaded counterparts. The loaded materials have tiny powder-like compounds scattered around, which could be the iron, calcium, and sulfur shown in the elemental spectrum. The SEM-EDS results are confirmed with FT-IR (Fig. SM7) and XRD analyses. As seen from the FT-IR, all the loaded materials show a distinctive peak at $\sim 1100\text{ cm}^{-1}$, which does not appear on the spectra of unloaded materials. This indicates the presence of P [75]. In addition, there are other peaks: $3500\text{--}3200\text{ cm}^{-1}$ can be assigned to -OH stretching vibrations and $1700\text{--}1500\text{ cm}^{-1}$ to C=O vibration [76]. There are also peaks between 500 and 700 cm^{-1} that correspond to the presence of iron [77, 78] or other metals, which can also be seen in the SEM-EDS spectra.

The XRF analysis (Fig. SM8) shows that the P fraction increases significantly for BC, BL, and LI but remains relatively the same for SC. However, looking at the XRF results together with the SEM-EDS and FT-IR results, the amount of P in the sample can increase despite the mass fraction of P not increasing. It is noteworthy that there is an absence of heavy metals in the loaded samples, highlighting the potency of these materials for agricultural applications [79]. However, the total heavy metal concentrations in the WWTP sludge where P was initially extracted were already below the legislative limits, so the purity of the loaded biosolids can partly be credited to the high-quality source material. (The wastewater sludge values in mg/kgTS were 0.42 for Hg, 0.44 for Cd, 28 for Cr, 300 for Cu, 14 for Pb, 17 for Ni, 490 for Zn, and 4 for Ar [39,40]. The respective limitations in Finnish fertilizer legislation in mg/kgTS are 1 for Hg, 1.5 for Cd, 300 for Cr, 600 for Cu, 100 for Pd, 100 for Ni, 1500 Zn, and 25 for Ar [79].)

XRD and XPS analyses were performed to understand the form of P adsorbed onto the tested adsorbents. Fig. 7 shows the XRD patterns of unloaded and loaded materials. The unloaded BL and SC have sodium present and seem to release it in the adsorption process while calcium is retained in the biomaterial. This indicates that P is bound to metals on the biosolid's surface, which is consistent with the good fit of the Hill isotherm model, suggesting that there is positive cooperative adsorption occurring. Yao et al. [80] showed that the presence of Mg improved P adsorption significantly. They did not find other metals, such as Fe or Ca, to have significance. However, the results of this study are not in agreement with that conclusion. The unloaded samples do not have identifiable P compounds, while the loaded BC and SC have FePO_4 and $\text{Ca}_{10}(\text{PO}_4)_6\text{Fe}_{0.45}\text{O}_2$, loaded BL has $\text{Ca}_4(\text{PO}_4)_2\text{O}$ and $\text{Fe}(\text{PO}_3)_2$, and LI has

$\text{Ca}_4(\text{PO}_4)_2\text{O}$ and $\text{Ca}_5(\text{PO}_4)_3(\text{CO}_3)_{0.5}$. These compounds reflect well with the elemental fractions shown in XRF and XPS results. Wang et al. [67] analyzed BC loaded with $\text{Ca}(\text{OH})_2$ and $\text{Ca}_5(\text{PO}_4)_3(\text{OH})$, which produced a roughly similar XRD pattern to the calcium species in LI and BL, where Ca species peaks are found across the spectrum. Similarly, Neeli and Ramsurn [81] observed several iron-related peaks ($2\theta \approx 40^\circ\text{--}50^\circ$), which corresponds to the Fe species identified in BL and LI. However, the biosolids in this study also had Fe species peaks between 20° and 30° . Furthermore, species with both Ca and Fe were also identified.

The authors did not observe precipitation reactions involving metals and phosphorus in the solution prior to adsorption test or while the solution was in cold storage. This indicates that the mechanism of adsorption occurred on the surface of the biosolid particles. Li and Stanforth [82] conclude that phosphate is adsorbed on goethite in low pH (3–4.5) as opposed to surface precipitation (pH 4.5–6). The goethite contains iron in its structure, whereas this study brought both dissolved P and Fe in contact with the biosolids. It is possible that first metal, Fe or Ca, is adsorbed on the surface of the biosolid and then phosphate follows. However, as both the solution and the biosolids were heterogenous materials with many different compounds, this effect is challenging to confirm in the scope of this P focused study. A dedicated study is required to examine metal-P interactions in heterogenous adsorption process.

XPS analysis was performed to analyze the stoichiometry and chemical bonding in the surface layers of both unloaded and loaded samples. The results are given as the relative composition of each sample in Table 5, as well as the survey spectra for the unloaded and loaded samples shown in Fig. 8. As can be seen from the survey spectra, all samples contained mostly carbon and oxygen before loading. High-resolution spectra from the C 1s region indicated that all unloaded samples, except unloaded BC, contained 50–65% aliphatic carbon (C-C bonding) and 20–35% carbon in C-O bonding. The unloaded BC sample showed typical graphitic bonding (C=C double bonds), exhibiting an asymmetric peak at 284.2 eV. After loading, all samples had C 1s spectra that were very similar to each other, with lower amounts of aliphatic carbon (approximately 45%) than the unloaded samples and with almost unchanged amounts of carbon in C-O bonding. All loaded samples contained considerably more carbon species at higher binding energies, which is associated with carbon-oxygen double bonds and carbon in carboxylic groups.

Apart from changes in the carbon chemistry, all loaded samples also exhibited considerably higher levels of phosphorous than their unloaded counterparts. No phosphorous content was detected on the unloaded samples, except for SC. After loading, all samples contained approximately 9–11% phosphorous, with the lowest amount at 9.3% for the loaded BL sample and the highest amount at 11.2% for the loaded BC sample, which is in agreement with the SEM-EDS results. However, the order of phosphorous content as measured by XPS might vary slightly with respect to the results obtained by other methods (such as SEM-EDS, due to a greater surface sensitivity for the method. High resolution spectra from the P 2p region were fitted $2p_{3/2}$ and $2p_{1/2}$ peaks, with an energy separation of 0.86 eV and a position of around $133.4\text{ eV} \pm 0.2\text{ eV}$ for the $2p_{3/2}$ peak. This binding energy would indicate that the phosphorous in the samples mainly exists in the form of phosphate, which is in agreement with the species identification by XRD. In addition to higher phosphorous content, all loaded samples also contained higher relative concentrations of oxygen (approximately 50%), as well as trace amounts of sulfur, calcium, iron, and nitrogen. The Fe 2p spectra showed asymmetric $2p_{3/2}$ peaks located at an energy of approximately $712.0\text{ eV} \pm 0.4\text{ eV}$. This energy would indicate that iron in the samples is in a Fe (III) oxidation state, most likely corresponding to Fe_2O_3 . A study by Wei et al. [83] showed that ZnO transforms to $\text{Zn}_3(\text{PO}_4)_2$. Similar reaction is possible with Fe in this study.

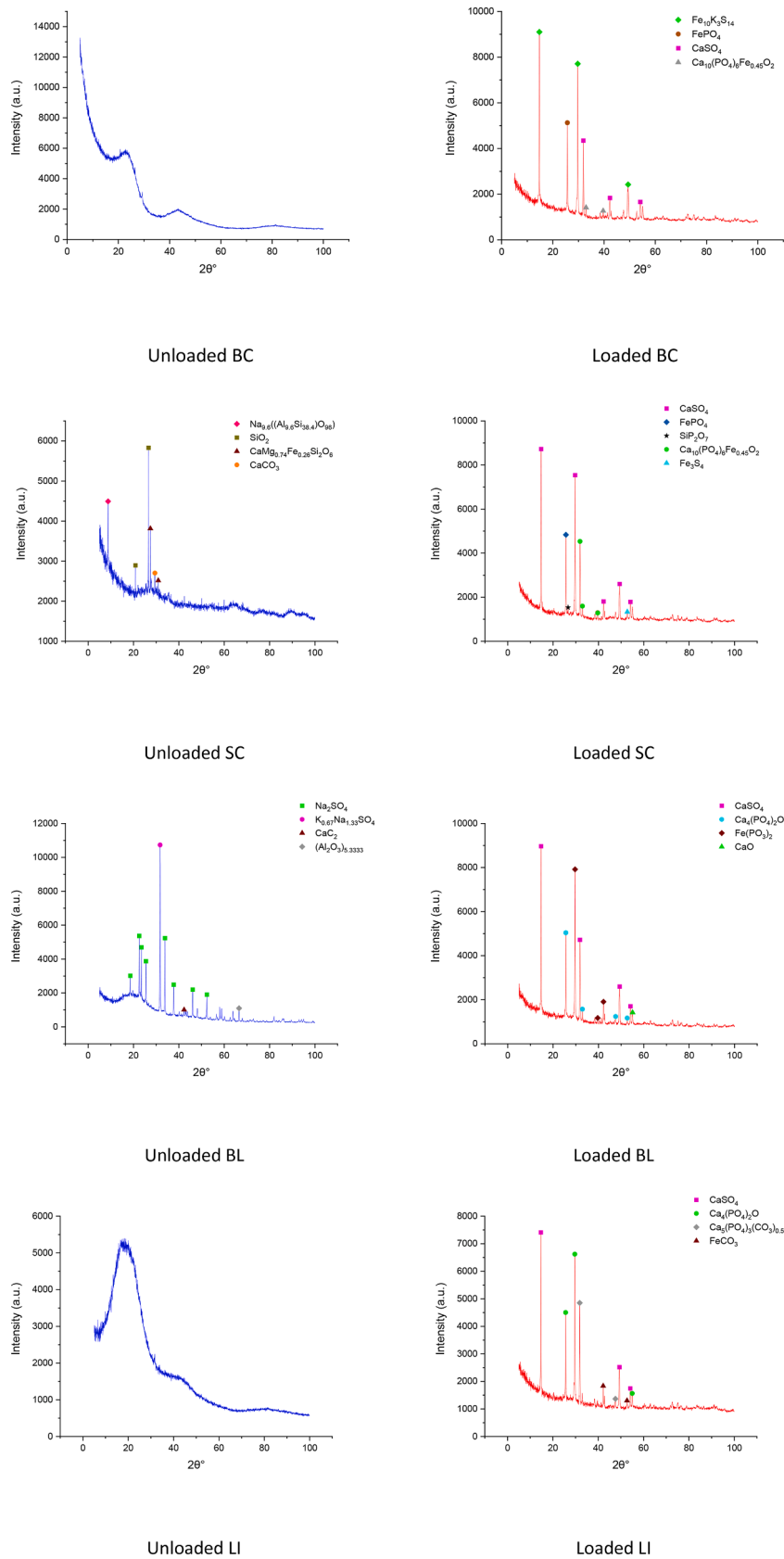


Fig. 7. XRD pattern of the loaded and unloaded biosolids.

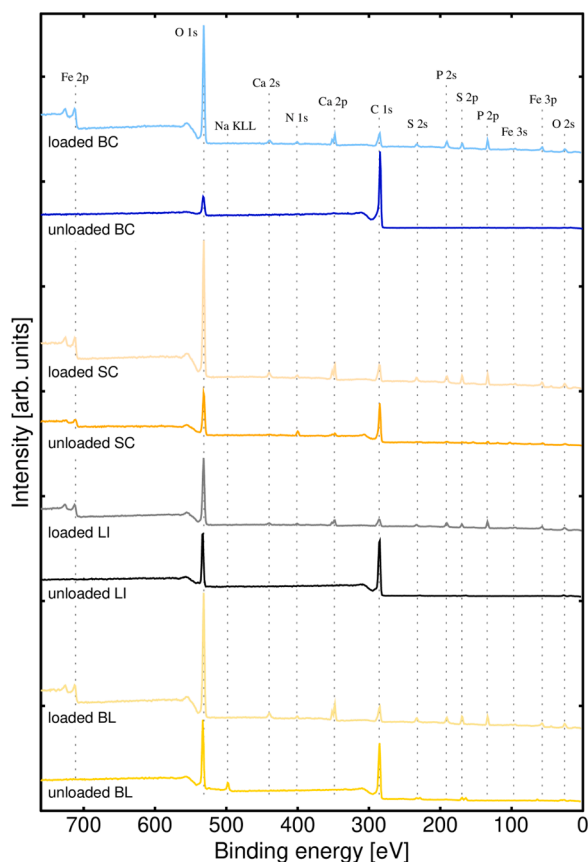


Fig. 8. XPS survey spectra for unloaded and loaded samples. Peak positions for all elements found in the samples are shown with dotted lines.

4. The potential of P-loaded biosolids as fertilizer

There are several quick methods used to estimate the P bioavailability [84]. The authors selected to use citric acid as extracting solution. Wang et al. [64] studied P extraction from biochar with citric acid. They reported that the extracted P fraction from Al loaded biochar was 15–18%. In this study, approximately 30% of the P was extracted from all biosolid materials in the extraction test. The PO_4^{3-} concentration in the post extraction solution was 91 mg/l for BC, 88 mg/l for LI, 91 mg/l for SC and 87 mg/l for BL after 30 min contact time with 2% citric acid. This indicates that P from our biosolids laced with Fe and Ca release a fraction of P readily but retain a greater fraction to be released slower.

However, a simple solubility test does not simulate the fertilizers' effect on plant growth [85,86]. To evaluate the fertilizing effect more accurately, other publications with cultivation studies were evaluated. Based on the experiments of Yao et al. [28] and Khan et al. [18], the estimated release time for P bound on biosolids is a few days. Yao et al. [28] performed a simple growth test with Mg-loaded BC and grass seedlings, showing that the loaded BC increased the growth test performance significantly compared to the control group. Khan et al. [18] prepared a loaded BC NPK fertilizer pellet but without the presence of metals and with a faster release time than that reported by Yao et al. [18]. Arun et al. [66] reported that their BC loaded with both P and N increased the biomass growth and chlorophyll count more than diammonium phosphate (DAP). Li et al. [33] made a simple but helpful estimation of the slow-release behavior of their Fe-loaded LI material. Within 30 days, the material released almost 70% of its Fe and P to water. Such biosolids in the soil can release the nutrients bound on them but also slowly degrade with biological activity [15] This further ensures nutrient release from BC and LI while maintaining soil health.

Discussing the two other biomaterials is more challenging since they

are novel and no existing literature can be found. However, they released P in equal quantity in 2% citric acid extraction test indicating that they will function as fertilizer in similar fashion. SC is carbonous material containing some level of metals, e.g., Fe and Ca present in its structure. The release rate of the nutrients might arguably be similar to that of BC. A general risk with char produced from sludge is the presence of heavy metals, which makes its use for agriculture questionable. However, the WWTP sludge used at the pyrolysis plant has acceptable heavy metal concentrations [39,40,78], thus the SC also is acceptable and safe to use. On the other hand, BL is the least porous material with a low surface area. It exchanges its sodium mass fraction with metals and P, and it is most likely closest to LI as an organic carbon structure. Thus, using BL as a fertilizer that degrades in soil should work as well as LI. However, these estimations need to be confirmed in an in-depth cultivation study.

5. Conclusions

One commercial and three waste-based biosolid materials—namely, biochar (BC) as a pure carbon source, lignin (LI) and humus extracted from black liquor (BL) as industrial side streams, and sludge char (SC) as a waste-turned-to-value product—were tested for P adsorption after P was leached off from municipal wastewater treatment sludge. BC, SC, LI, and BL were compared in terms of P adsorption efficiency, adsorption mechanisms, P species, and solid structure. SC performed the best, while BC performed the poorest in terms of adsorption capacity (q). The typical values for q ranged from 100 mg/g to 200 mg/g in room temperature, but the highest values were 400–500 mg/g adsorbent at 40°C. The solution after P extraction from sludge contains Fe, Ca, and S, which also bind to the solid materials. The main form of P on the solid material was phosphate, and it was bound with Fe or Ca. No heavy metals were detected on the loaded biomaterials. Kinetic adsorption models showed that all biomaterials obey the PFO model. The isotherm models (the Hill model being the best fitting) suggest a positive cooperative adsorption process between the species in the leachate with both pore and intraparticle diffusion affecting the process. The process is endothermic. The phosphorus adsorbed onto the materials proved to be phosphate bound with Fe and Ca. Therefore, the examined biosolids point towards a sustainable solution as slow-release fertilizers.

Funding information

This work was supported by Maa- ja Vesitekniikan tuki ry (MVTT) with 48 000 €. MVTT is a Finnish funding organization dedicated to support research and inventions in the field of water and environmental technology. They also support projects that relate to soil protection, agricultural planning and construction.

MVTT had no role in the study design, data collection, analysis or interpretation. Furthermore, MVTT did not participate in the writing of the report nor were they involved in the article for publication.

Declaration of Competing Interests

The authors declare that they have no known competing financial interests or personal relationships that could have appeared to influence the work reported in this paper. The authors declare the following

Table 1
Surface area and porosity results for raw biomaterials.

Material	Total pore volume ($\text{cm}^3 \text{g}^{-1}$)	Mean pore diameter (nm)	Surface area $\text{m}^2 \text{g}^{-1}$
BC	0.107	2.266	33.726
SC	0.082	39.500	8.822
LI	0.026	43.464	2.189
BL	0.003	12.003	0.897

Table 2

Parameters derived from kinetic models.

	PFO			PSO		
	k_1	q_e	R^2	k_2	q_e	R^2
BC	0.04 ± 0.003	43.0 ± 0	0.96	0.002 ± 5.8E-4	43.0 ± 0	0.94
BL	0.03 ± 0.003	43.0 ± 3.5	0.98	-1.9E15 ± 0	43.6 ± 4.7	0.78
LI	0.03 ± 0.002	37.5 ± 2.6	0.99	-1.2E14 ± 0	41.7 ± 3.1	0.91
SC	0.07 ± 0.006	64.5 ± 16.9	0.97	-3.3E19 ± 0	48.3 ± 5.0	0.79

Table 3

Fitting performance for the intraparticle diffusion model.

		Intraparticle diffusion		Boyd model	
		Single linear fit	Piecewise linear fit		
BC	R-Square (COD)	0.98	0.99	0.99	0.99
	Adj. R-Square	0.97	0.99	0.99	0.99
LI	R-Square (COD)	0.92	0.96	0.96	0.92
	Adj. R-Square	0.91	0.92	0.92	0.91
SC	R-Square (COD)	0.92	0.98	0.98	0.97
	Adj. R-Square	0.91	0.97	0.97	0.96
BL	R-Square (COD)	0.96	0.98	0.98	0.99
	Adj. R-Square	0.95	0.96	0.96	0.99

Table 4

Free energy change results for all biomaterials

	ΔG^0 (kJ/mole)				ΔH^0 (kJ/mole)	ΔS^0 (J/mole/°K)
	10°C	20°C	30°C	40°C		
BL	-6,756.06	-6,994.66	-7,233.26	-7,471.87	24.15	-7,066.60
LI	-6,783.13	-7,022.69	-7,262.25	-7,501.81	22.23	-6,492.20
SC	-6,795.61	-7,035.61	-7,275.61	-7,515.61	22.63	-6,624.40
BC	-6,293.95	-6,516.23	-6,738.51	-6,960.80	20.48	-6,020.50

Table 5

The relative composition of unloaded and loaded samples, as measured by XPS.

	C %	O %	S %	P %	Ca %	Fe %	N %	Na %
BC	91.3	8.7	-	-	-	-	-	-
BC-loaded	23.1	52.0	4.2	11.2	3.3	4.2	1.9	-
LI	79.1	20.1	0.7	-	-	-	-	-
LI-loaded	22.9	51.7	4.9	10.8	4.0	3.6	2.0	-
SC	65.4	24.3	1.1	2.4	1.3	1.1	4.3	-
SC-loaded	27.9	48.9	4.9	9.8	3.9	2.9	1.7	-
BL	71.4	23.9	3.8	-	-	-	-	0.9
BL-loaded	22.3	51.5	6.6	9.3	5.2	3.6	1.6	-

financial interests/personal relationships which may be considered as potential competing interests:

Acknowledgments

This work was supported by Maa- ja Vesiteknikaan tuki ry (MVTT). Furthermore, special thank you for Aino Peltola for assistance in laboratory analyses.

Supplementary materials

Supplementary material associated with this article can be found, in the online version, at [doi:10.1016/j.cej.2022.100329](https://doi.org/10.1016/j.cej.2022.100329).

References

- [1] D. Cordell, J.-O. Drangert, S. White, The story of phosphorus: Global food security and food for thought, *Global Environmental Change* 19 (2) (2009) 292–305, <https://doi.org/10.1016/j.gloenvcha.2008.10.009>. May.
- [2] J.D. Edixhoven, J. Gupta, H.H.G. Savenije, Recent revisions of phosphate rock reserves and resources: a critique, *Earth Syst. Dynam.* 5 (2) (2014) 491–507, <https://doi.org/10.5194/esd-5-491-2014>. Dec.
- [3] R.W. Scholz, F.-W. Wellmer, Comment on: “Recent revisions of phosphate rock reserves and resources: a critique” by Edixhoven et al. (2014) – clarifying comments and thoughts on key conceptions, conclusions and interpretation to allow for sustainable action, *Earth Syst. Dynam.* 7 (1) (2016) 103–117, <https://doi.org/10.5194/esd-7-103-2016>. Feb.
- [4] P. Walan, S. Davidsson, S. Johansson, M. Höök, Phosphate rock production and depletion: Regional disaggregated modeling and global implications, *Resources, Conservation and Recycling* 93 (2014) 178–187, <https://doi.org/10.1016/j.resconrec.2014.10.011>. Dec.
- [5] J. J. Schröder, W. U. and R. Centre, D. Cordell, A. L. Smit, and A. Rosemarin, “Sustainable use of phosphorus: EU tender ENV.B1/ETU/2009/0025,” Wageningen (Netherlands) Plant Research International, 2010. Accessed: Oct. 05, 2021. [Online]. Available: <http://edepot.wur.nl/163942>.
- [6] G. Mininni, A.R. Blanch, F. Lucena, S. Berselli, EU policy on sewage sludge utilization and perspectives on new approaches of sludge management, *Environ Sci Pollut Res* 22 (10) (2015) 7361–7374, <https://doi.org/10.1007/s11356-014-3132-0>. May.
- [7] M. Prud’homme, *World Phosphate Rock Flows, Losses and Uses, Phosphates 2010 International Conference (2010) 22–24. March Brussels.* International Fertilizer Industry Association.
- [8] J. Huang, C. Xu, B.G. Ridoutt, X. Wang, P. Ren, Nitrogen and phosphorus losses and eutrophication potential associated with fertilizer application to cropland in China, *Journal of Cleaner Production* 159 (2017) 171–179, <https://doi.org/10.1016/j.jclepro.2017.05.008>. Aug.
- [9] D.F. Leikam, F.P. Achorn, *Phosphate Fertilizers: Production, Characteristics, and Technologies, Phosphorus: Agriculture and the Environment*, John Wiley & Sons, Ltd (2015) 23–50, <https://doi.org/10.2134/agronmonogr46.c2>.
- [10] S. Kratz, C. Vogel, C. Adam, Agronomic performance of P recycling fertilizers and methods to predict it: a review, *Nutr Cycl Agroecosyst* 115 (1) (2019) 1–39, <https://doi.org/10.1007/s10705-019-10010-7>. Sep.
- [11] M. Hedley, M. McLaughlin, *Reactions of Phosphate Fertilizers and By-Products in Soils, Phosphorus: Agriculture and the Environment* (2005) 181–252, <https://doi.org/10.2134/agronmonogr46.c7>.
- [12] Y. Fodoue, N. Jean Pierre, R. Tchameni, S. Basga, J. Penaye, Assessment of the Fertilizing effect of Vivianite on the Growth and yield of the Bean “phaseolus vulgaris” on Oxisols from Ngaoundere (Central North Cameroon, *International Research Journal of Earth Sciences* 3 (2015) 18–26. Mar.
- [13] H.-D. Ryu, C.-S. Lim, Y.-K. Kim, K.-Y. Kim, S.-I. Lee, Recovery of Struvite Obtained from Semiconductor Wastewater and Reuse as a Slow-Release Fertilizer, *Environmental Engineering Science* 29 (6) (2012) 540–548, <https://doi.org/10.1089/ees.2011.0207>. Jun.
- [14] P. J. A. Withers and M. J. Bowes, “Phosphorus the pollutant,” in *Phosphorus: Polluter and Resource of the Future – Removal and Recovery from Wastewater*, C. Schaum, Ed. International Water Association, 2018, pp. 1–33. doi: 10.2166/9781780408361_003.
- [15] G.C. Chen, Z.L. He, P.J. Stoffella, X.E. Yang, S. Yu, D. Calvert, Use of dolomite phosphate rock (DPR) fertilizers to reduce phosphorus leaching from sandy soil, *Environmental Pollution* 139 (1) (Jan. 2006) 176–182, <https://doi.org/10.1016/j.envpol.2004.12.016>.
- [16] A.K. Bansawal, S.S. Rayalu, N.K. Labhasetwar, A.A. Juwarkar, S. Devotta, Surfactant-Modified Zeolite as a Slow Release Fertilizer for Phosphorus, *J. Agric. Food Chem.* 54 (13) (2006) 4773–4779, <https://doi.org/10.1021/jf060034b>. Jun.
- [17] R. Azlinawati Ramli, Slow release fertilizer hydrogels: a review, *Polymer Chemistry* 10 (45) (2019) 6073–6090, <https://doi.org/10.1039/C9PY01036J>.
- [18] M.A. Khan, K.-W. Kim, W. Mingzhi, B.-K. Lim, W.-H. Lee, J.-Y. Lee, Nutrient-impregnated charcoal: an environmentally friendly slow-release fertilizer, *Environmentalist* 28 (3) (2008) 231–235, <https://doi.org/10.1007/s10669-007-9133-5>. Sep.
- [19] R. Lal, Soil health and carbon management, *Food and Energy Security* 5 (4) (2016) 212–222, <https://doi.org/10.1002/fes3.96>.
- [20] D. Woolf, J.E. Amonette, F.A. Street-Perrott, J. Lehmann, S. Joseph, Sustainable biochar to mitigate global climate change, *Nat Commun* 1 (1) (2010) 56, <https://doi.org/10.1038/ncomms1053>. Aug.
- [21] J. Lehmann, A handful of carbon, *Nature* 447 (7141) (2007) 143–144, <https://doi.org/10.1038/447143a>. May.
- [22] E. Marris, Black is the new green, *Nature* 442 (7103) (2006) 624–626, <https://doi.org/10.1038/442624a>. Aug.
- [23] M.R. Yazdani, et al., Dataset for natural organic matter treatment by tailored biochars, *Data in Brief* 25 (2019), 104353, <https://doi.org/10.1016/j.dib.2019.104353>. Aug.
- [24] M.R. Yazdani, et al., Tailored mesoporous biochar sorbents from pinecone biomass for the adsorption of natural organic matter from lake water, *Journal of Molecular Liquids* 291 (2019), 111248, <https://doi.org/10.1016/j.molliq.2019.111248>. Oct.
- [25] O. Tomin, R. Vahala, M.R. Yazdani, Tailoring metal-impregnated biochars for selective removal of natural organic matter and dissolved phosphorus from the aqueous phase, *Microporous and Mesoporous Materials* 328 (Dec. 2021), 111499, <https://doi.org/10.1016/j.micromeso.2021.111499>.

- [26] H. Yang, et al., Utilization of biochar for resource recovery from water: A review, *Chemical Engineering Journal* 397 (Oct. 2020), 125502, <https://doi.org/10.1016/j.cej.2020.125502>.
- [27] W. Xiang, et al., Biochar technology in wastewater treatment: A critical review, *Chemosphere* 252 (2020), 126539, <https://doi.org/10.1016/j.chemosphere.2020.126539>. Aug.
- [28] Y. Yao, et al., Engineered carbon (biochar) prepared by direct pyrolysis of Mg-accumulated tomato tissues: Characterization and phosphate removal potential, *Bioresource Technology* 138 (2013) 8–13, <https://doi.org/10.1016/j.biortech.2013.03.057>. Jun.
- [29] J. Chen, X. Fan, L. Zhang, X. Chen, S. Sun, R. Sun, Research Progress in Lignin-Based Slow/Controlled Release Fertilizer, *ChemSusChem* 13 (17) (2020) 4356–4366, <https://doi.org/10.1002/cssc.202000455>. Sep.
- [30] X. Liu, et al., Lignin-Derived Porous Carbon Loaded with La(OH)₃ Nanorods for Highly Efficient Removal of Phosphate, *ACS Sustainable Chem. Eng.* 7 (1) (2019) 758–768, <https://doi.org/10.1021/acsschemeng.8b04382>. Jan.
- [31] T. Han, X. Lu, Y. Sun, J. Jiang, W. Yang, P.G. Jönsson, Magnetic bio-activated carbon production from lignin via a streamlined process and its use in phosphate removal from aqueous solutions, *Science of The Total Environment* 708 (2020), 135069, <https://doi.org/10.1016/j.scitotenv.2019.135069>. Mar.
- [32] A. Li, H. Deng, Y. Wu, C. Ye, Y. Jiang, Strong Adsorption of Phosphorus by ZnAl-LDO-Activated Banana Biochar: An Analysis of Adsorption Efficiency, Thermodynamics, and Internal Mechanisms, *ACS Omega* 6 (11) (2021) 7402–7412, <https://doi.org/10.1021/acsomega.0c05674>. Mar.
- [33] T. Li, et al., Fabrication of a Lignin-Based Magnetic Nanocomposite Adsorbent to Recover Phosphorus in Water for Agricultural Reuse, *ACS Sustainable Chem. Eng.* 9 (31) (2021) 10468–10478, <https://doi.org/10.1021/acsschemeng.1c01492>. Aug.
- [34] G.-J. Jiao, et al., Recent advances and challenges on removal and recycling of phosphate from wastewater using biomass-derived adsorbents, *Chemosphere* 278 (2021), 130377, <https://doi.org/10.1016/j.chemosphere.2021.130377>. Sep.
- [35] Q. Yang, et al., Effectiveness and mechanisms of phosphate adsorption on iron-modified biochars derived from waste activated sludge, *Bioresource Technology* 247 (2018) 537–544, <https://doi.org/10.1016/j.biortech.2017.09.136>. Jan.
- [36] Q.-X. Hua, J.-Y. Li, J.-M. Zhou, H.-Y. Wang, C.-W. Du, X.-Q. Chen, Enhancement of Phosphorus Solubility by Humic Substances in Ferrosols, *Pedosphere* 18 (4) (2008) 533–538, [https://doi.org/10.1016/S1002-0160\(08\)60044-2](https://doi.org/10.1016/S1002-0160(08)60044-2). Aug.
- [37] A. Delgado, A. Madrid, S. Kassem, L. Andreu, M. del Carmen del Campillo, Phosphorus fertilizer recovery from calcareous soils amended with humic and fulvic acids, *Plant and Soil* 245 (2) (2002) 277–286, <https://doi.org/10.1023/A:1020445710584>. Aug.
- [38] J. Uzkurt Kaljunen, R.A. Al-Juboori, A. Mikola, I. Righetto, I. Konola, Newly developed membrane contactor-based N and P recovery process: Pilot-scale field experiments and cost analysis, *Journal of Cleaner Production* 281 (2021), 125288, <https://doi.org/10.1016/j.jclepro.2020.125288>. Jan.
- [39] HSY, “Jätevedenpuhdistus pääkaupunkiseudulla 2018,” 2018. <https://julkaisu.hsy.fi/jatevedenpuhdistus-paakaupunkiseudulla-2018.html> (accessed May 31, 2021).
- [40] HSY, “Jätevedenpuhdistus pääkaupunkiseudulla 2019,” <https://julkaisu.hsy.fi/jatevedenpuhdistus-paakaupunkiseudulla-2019.html> (accessed Oct. 28, 2021).
- [41] V.(Vusie) Mema, Identification of extraction methods for the production of humic acids from black liquor, Thesis, Stellenbosch: University of Stellenbosch (2006). Accessed: May 31, 2021. [Online]. Available: <https://scholar.sun.ac.za:443/handle/10019.1/3059>.
- [42] W. Jia, S. Ren, B. Hu, Effect of Water Chemistry on Zeta Potential of Air Bubbles, *International Journal of Electrochemical Science* 8 (2013) 5828–5837. Apr.
- [43] X. Tong, J. Li, J. Yuan, R. Xu, Adsorption of Cu(II) by biochars generated from three crop straws, *Chemical Engineering Journal* 172 (2) (2011) 828–834, <https://doi.org/10.1016/j.cej.2011.06.069>. Aug.
- [44] M. Rezakazemi, S. Shirazian, Lignin-chitosan blend for methylene blue removal: Adsorption modeling, *Journal of Molecular Liquids* 274 (2019) 778–791, <https://doi.org/10.1016/j.molliq.2018.11.043>. Jan.
- [45] H. Qiu, L. Lv, B. Pan, Q. Zhang, W. Zhang, Q. Zhang, Critical review in adsorption kinetic models, *J. Zhejiang Univ. Sci. A* 10 (5) (2009) 716–724, <https://doi.org/10.1631/jzus.A0820524>. May.
- [46] K.L. Tan, B.H. Hameed, Insight into the adsorption kinetics models for the removal of contaminants from aqueous solutions, *Journal of the Taiwan Institute of Chemical Engineers* 74 (2017) 25–48, <https://doi.org/10.1016/j.jtice.2017.01.024>. May.
- [47] S.S.A. Alkurd, R.A. Al-Juboori, J. Bundschuh, L. Bowtell, A. Marchuk, Inorganic arsenic species removal from water using bone char: A detailed study on adsorption kinetic and isotherm models using error functions analysis, *Journal of Hazardous Materials* 405 (2021), 124112, <https://doi.org/10.1016/j.jhazmat.2020.124112>. Mar.
- [48] J. Wang, X. Guo, Adsorption isotherm models: Classification, physical meaning, application and solving method, *Chemosphere* 258 (2020), 127279, <https://doi.org/10.1016/j.chemosphere.2020.127279>. Nov.
- [49] K.Y. Foo, B.H. Hameed, Insights into the modeling of adsorption isotherm systems, *Chemical Engineering Journal* 156 (1) (2010) 2–10, <https://doi.org/10.1016/j.cej.2009.09.013>. Jan.
- [50] O.A. Dada, A.P. Olalekan, A.M. Olatunya, O. Dada, Langmuir, Freundlich, Temkin and Dubinin–Radushkevich Isotherms Studies of Equilibrium Sorption of Zn 2+ Unto Phosphoric Acid Modified Rice Husk, *IOSRJC* 3 (1) (2012) 38–45, <https://doi.org/10.9790/5736-0313845>.
- [51] M.J. Ahmed, S.K. Dhedan, Equilibrium isotherms and kinetics modeling of methylene blue adsorption on agricultural wastes-based activated carbons, *Fluid Phase Equilibria* 317 (2012) 9–14, <https://doi.org/10.1016/j.fluid.2011.12.026>. Mar.
- [52] R. Saadi, Z. Saadi, R. Fazaeli, N.E. Fard, Monolayer and multilayer adsorption isotherm models for sorption from aqueous media, *Korean J. Chem. Eng.* 32 (5) (2015) 787–799, <https://doi.org/10.1007/s11814-015-0053-7>. May.
- [53] H. Shahbeig, N. Bagheri, S.A. Ghorbanian, A. Hallajisani, S. Poorkarimi, A new adsorption isotherm model of aqueous solutions on granular activated carbon, *World Journal of Modelling and Simulation* 9 (4) (2013) 12.
- [54] S.J. Salih, S.S. Anwer, R.H. Faraj, A Biosorption of Mercury from Wastewater Using Isolated *Aspergillus* Sp. Modified 1,10-Phenanthroline: Hill Isotherm Model, *Science Journal of University of Zakho* 5 (4) (2017) 4, <https://doi.org/10.25271/2017.5.4.379>. Art. noDec.
- [55] Q. Hu, Z. Zhang, Application of Dubinin–Radushkevich isotherm model at the solid/solution interface: A theoretical analysis, *Journal of Molecular Liquids* 277 (2019) 646–648, <https://doi.org/10.1016/j.molliq.2019.01.005>. Mar.
- [56] E. Wiedenbeck, D. Gebauer, H. Cölfen, Potentiometric Titration Method for the Determination of Solubility Limits and pKa Values of Weak Organic Acids in Water, *Anal. Chem.* 92 (14) (2020) 9511–9515, <https://doi.org/10.1021/acs.analchem.0c00247>. Jul.
- [57] K. Vijayaraghavan, T. Padmesh, K. Palanivelu, M. Velan, Biosorption of nickel(II) ions onto *Sargassum wightii*: Application of two-parameter and three-parameter isotherm models, *Journal of Hazardous Materials* 133 (1–3) (2006) 304–308, <https://doi.org/10.1016/j.jhazmat.2005.10.016>. May.
- [58] Y.S. Ho, J.F. Porter, G. McKay, Equilibrium Isotherm Studies for the Sorption of Divalent Metal Ions onto Peat: Copper, Nickel and Lead Single Component Systems, *Water, Air, & Soil Pollution* 141 (1) (2002) 1–33, <https://doi.org/10.1023/A:1021304828010>. Nov.
- [59] T.V.N. Padmesh, K. Vijayaraghavan, G. Sekaran, M. Velan, Application of Two- and Three-Parameter Isotherm Models: Biosorption of Acid Red 88 onto *Azolla microphylla*, *Bioremediation Journal* 10 (2006) 37–44, 1/2Jun.
- [60] H. Li, G. Huang, C. An, J. Hu, S. Yang, Removal of Tannin from Aqueous Solution by Adsorption onto Treated Coal Fly Ash: Kinetic, Equilibrium, and Thermodynamic Studies, *Ind. Eng. Chem. Res.* 52 (45) (2013) 15923–15931, <https://doi.org/10.1021/ie402054w>. Nov.
- [61] M.Roza Yazdani, T. Tuutijärvi, A. Bhatnagar, R. Vahala, Adsorptive removal of arsenic(V) from aqueous phase by feldspars: Kinetics, mechanism, and thermodynamic aspects of adsorption, *Journal of Molecular Liquids* 214 (Feb. 2016) 149–156, <https://doi.org/10.1016/j.molliq.2015.12.002>.
- [62] C. Valderrama, X. Gamisans, X. de las Heras, A. Farrán, J.L. Cortina, Sorption kinetics of polycyclic aromatic hydrocarbons removal using granular activated carbon: Intraparticle diffusion coefficients, *Journal of Hazardous Materials* 157 (2) (2008) 386–396, <https://doi.org/10.1016/j.jhazmat.2007.12.119>. Sep.
- [63] M.I. El-Khaiy, G.F. Malash, Common data analysis errors in batch adsorption studies, *Hydrometallurgy* 105 (3) (2011) 314–320, <https://doi.org/10.1016/j.hydromet.2010.11.005>. Jan.
- [64] T. Wang, M. Camps-Arbestain, M. Hedley, P. Bishop, Predicting phosphorus bioavailability from high-ash biochars, *Plant Soil* 357 (2012) 173–187, <https://doi.org/10.1007/s11104-012-1131-9>.
- [65] S. Ma, F. Jing, S.P. Sohi, J. Chen, New insights into contrasting mechanisms for PAE adsorption on millimeter, micron- and nano-scale biochar, *Environ Sci Pollut Res* 26 (2019) 18636–18650, <https://doi.org/10.1007/s11356-019-05181-3>.
- [66] J. Arun, K.P. Gopinath, S.S. Vigneshwar, A. Swetha, Sustainable and eco-friendly approach for phosphorus recovery from wastewater by hydrothermally carbonized microalgae: Study on spent bio-char as fertilizer, *Journal of Water Process Engineering* 38 (2020), 101567, <https://doi.org/10.1016/j.jwpe.2020.101567>. Dec.
- [67] S. Wang, et al., Adsorption of phosphorus by calcium-flour biochar: Isotherm, kinetic and transformation studies, *Chemosphere* 195 (2018) 666–672, <https://doi.org/10.1016/j.chemosphere.2017.12.101>. Mar.
- [68] X. Li, J. Shi, Simultaneous adsorption of tetracycline, ammonium and phosphate from wastewater by iron and nitrogen modified biochar: Kinetics, isotherm, thermodynamic and mechanism, *Chemosphere* 293 (2022), 133574, <https://doi.org/10.1016/j.chemosphere.2022.133574>.
- [69] E. Cussler, Chapter 15. Adsorption, in E. Cussler, *Diffusion: Mass Transfer in Fluid Systems* (3rd ed., Cambridge Series in Chemical Engineering), Cambridge University Press, Cambridge, 2009, <https://doi.org/10.1017/CBO9780511805134>.
- [70] L.K. Koopal, W.H. van Riemsdijk, J.C.M. de Wit, M.F. Benedetti, Analytical Isotherm Equations for Multicomponent Adsorption to Heterogeneous Surfaces, *Journal of Colloid and Interface Science* 166 (1) (1994) 51–60, <https://doi.org/10.1006/jcis.1994.1270>. Aug.
- [71] D. Ringot, B. Lerzy, K. Chaplain, J.-P. Bonhoure, E. Auclair, Y. Larondelle, In vitro biosorption of ochratoxin A on the yeast industry by-products: Comparison of isotherm models, *Bioresource Technology* 98 (9) (2007) 1812–1821, <https://doi.org/10.1016/j.biortech.2006.06.015>. Jul.
- [72] F. Gimbert, N. Morin-Crini, F. Renault, P.-M. Badot, G. Crini, Adsorption isotherm models for dye removal by cationized starch-based material in a single component system: Error analysis, *Journal of Hazardous Materials* 157 (1) (2008) 34–46, <https://doi.org/10.1016/j.jhazmat.2007.12.072>. Aug.
- [73] A.B. Pérez-Marín, V.M. Zapata, J.F. Ortuño, M. Aguilar, J. Sáez, M. Lloréns, Removal of cadmium from aqueous solutions by adsorption onto orange waste, *Journal of Hazardous Materials* 139 (1) (2007) 122–131, <https://doi.org/10.1016/j.jhazmat.2006.06.008>. Jan.
- [74] M.H. Mahaninia, L.D. Wilson, Cross-linked chitosan beads for phosphate removal from aqueous solution, *Journal of Applied Polymer Science* 133 (5) (2016), <https://doi.org/10.1002/app.42949>.

- [75] R. Karunanithi, et al., Sorption, kinetics and thermodynamics of phosphate sorption onto soybean stover derived biochar, *Environmental Technology & Innovation* 8 (2017) 113–125, <https://doi.org/10.1016/j.eti.2017.06.002>. Nov.
- [76] C. Fang, T. Zhang, P. Li, R. Jiang, and Y. Wang, "Application of Magnesium Modified Corn Biochar for Phosphorus Removal and Recovery from Swine Wastewater," *International Journal of Environmental Research and Public Health*, vol. 11, no. 9, Art. no. 9, Sep. 2014, doi: 10.3390/ijerph110909217.
- [77] H. Liu, X. Sun, C. Yin, C. Hu, Removal of phosphate by mesoporous ZrO₂, *Journal of Hazardous Materials* 151 (2) (2008) 616–622, <https://doi.org/10.1016/j.jhazmat.2007.06.033>. Mar.
- [78] K. Phoungthong, T. Suwunwong, Magnetic biochar derived from sewage sludge of concentrated natural rubber latex (CNRL) for the removal of Al³⁺ and Cu²⁺ ions from wastewater, *Res Chem Intermed* 46 (1) (2020) 385–407, <https://doi.org/10.1007/s11164-019-03956-4>. Jan.
- [79] Ruokavirasto, Haitalliset aineet ja hygienia, Ruokavirasto (2021) <https://www.ruokavirasto.fi/yritykset/rehu-ja-lannoiteala/lannoitevalmisteet/laatuvaatimukset/haitalliset-aineet-ja-hygienia/> (accessed Oct. 28, 2021).
- [80] Y. Yao, B. Gao, J. Chen, L. Yang, Engineered Biochar Reclaiming Phosphate from Aqueous Solutions: Mechanisms and Potential Application as a Slow-Release Fertilizer, *Environ. Sci. Technol.* 47 (15) (2013) 8700–8708, <https://doi.org/10.1021/es4012977>. Aug.
- [81] S.T. Neeli, H. Ramsurn, Synthesis and formation mechanism of iron nanoparticles in graphitized carbon matrices using biochar from biomass model compounds as a support, *Carbon* 134 (2018) 480–490, <https://doi.org/10.1016/j.carbon.2018.03.079>. Aug.
- [82] L. Li, R. Stanforth, Distinguishing Adsorption and Surface Precipitation of Phosphate on Goethite (α -FeOOH), *Journal of Colloid and Interface Science* 230 (2000) 12–21, <https://doi.org/10.1006/jcis.2000.7072>.
- [83] Y. Wei, X. Liang, H. Wu, J. Cen, Y. Ji, Efficient phosphate removal by dendrite-like halloysite-zinc oxide nanocomposites prepared via noncovalent hybridization, *Applied Clay Science* 213 (2021), 106232, <https://doi.org/10.1016/j.clay.2021.106232>.
- [84] T.J. Mattila, J. Rajala, Do different agronomic soil tests identify similar nutrient deficiencies? *Soil Use and Management* 38 (2022) 635–648, <https://doi.org/10.1111/sum.12738>.
- [85] M. Hedley, M. McLaughlin, Reactions of phosphate fertilizers and by-products in soils. *Phosphorus: Agriculture and the Environment*, American Society of Agronomy, Madison, Wis, 2005, pp. 217–230.
- [86] S. Kratz, C. Vogel, C. Adam, Agronomic performance of P recycling fertilizers and methods to predict it: a review, *Nutr Cycl Agroecosyst* 115 (2019) 1–39, <https://doi.org/10.1007/s10705-019-10010-7>.